Magnetic fields and differential rotation on the pre-main sequence - III. The early-G star HD 106506

I. A. Waite, S. C. Marsden, B. D. Carter, R. Hart, Jean-François Donati, J. C. Rámirez Vélez, Meir Semel, N. J. Dunstone

Monthly Notices
of the
ROYAL ASTRONOMICAL SOCIETY

Mon. Not. R. Astron. Soc. **413,** 1949–1960 (2011) doi:10.1111/j.1365-2966.2011.18366.x

Magnetic fields and differential rotation on the pre-main sequence – III. The early-G star HD 106506

I. A. Waite,[1⋆] S. C. Marsden,[2,3] B. D. Carter,[1] R. Hart,[1] J.-F. Donati,[4] J. C. Ramírez Vélez,[5,6] M. Semel[4] and N. Dunstone[7]

[1] *Faculty of Sciences, University of Southern Queensland, Toowoomba 4350, Australia*
[2] *Australian Astronomical Observatory, PO Box 296, Epping, Sydney 1710, Australia*
[3] *Centre for Astronomy, School of Engineering and Physical Sciences, James Cook University, Townsville 4811, Australia*
[4] *LATT-UMR 5572, CNRS & Univ. de Toulouse, 14 Av. E. Belin, F-31400 Toulouse, France*
[5] *LESIA, Observatoire de Paris-Meudon, F-92195 Meudon Cedex, France*
[6] *Instituto de Astronomia, Universidad Nacional Autónoma de México, 04510 Coyoacon, México D.F*
[7] *SUPA, School of Physics and Astronomy, University of St Andrews, St Andrews KY16 9SS*

Accepted 2011 January 14. Received 2010 December 16; in original form 2010 March 15

ABSTRACT

We present the photometry and spectropolarimetry of the pre-main-sequence star HD 106506. A photometric rotational period of $\sim$1.416 $\pm$ 0.133 d has been derived using observations at Mount Kent Observatory (MKO). Spectropolarimetric data obtained with the 3.9-m Anglo-Australian Telescope (AAT) were used to derive spot occupancy and magnetic maps of the star through the technique of Zeeman Doppler imaging (ZDI). The resulting brightness maps indicate that HD 106506 displays photospheric spots at all latitudes including a predominant polar spot. Azimuthal and radial magnetic images of this star have been derived, and a significant azimuthal magnetic field is indicated, in line with other active young stars. A solar-like differential rotation law was incorporated into the imaging process. Using Stokes *I* information the equatorial rotation rate, $\Omega_{\rm eq}$, was found to be 4.54 $\pm$ 0.01 rad d^{-1}, with a photospheric shear $\delta\Omega$ of $0.21^{+0.02}_{-0.03}$ rad d^{-1}. This equates to an equatorial rotation period of $\sim$1.39 $\pm$ 0.01 d, with the equatorial region lapping the poles every $\sim 30^{+5}_{-3}$ d. Using the magnetic features, the equatorial rotation rate, $\Omega_{\rm eq}$, was found to be 4.51 $\pm$ 0.01 rad d^{-1}, with a photospheric shear $\delta\Omega$ of 0.24 $\pm$ 0.03 rad d^{-1}. This differential rotation is approximately four times that observed on the Sun.

Key words: line: profiles – stars: activity – stars: individual: HD 106506 – stars: magnetic field – stars: solar-type – starspots.

1 INTRODUCTION

Young solar-type F, G and K stars provide proxies for the Sun's early evolution and insight into its intense pre-main-sequence and zero-age main-sequence magnetic activity. In this regard, observations of star-spots and surface magnetic fields are important, as they provide the empirical basis for understanding the star's magnetic dynamo and its internal structure. Differential rotation is one of the primary drivers of the dynamo process that produces magnetic fields within the Sun. In the solar convection zone, differential rotation is constant down to the base of this zone in the region known as the tachocline. Strong shear forces are formed at the interface between the solid-body rotation of the radiative zone and the differentially rotating convective layer. This interaction converts the poloidal magnetic field to a toroidal field. This effect is known as the 'Ω-effect'. However, on young solar-type stars, the operation of the magnetic dynamo process may be occurring throughout the convective zone itself. This is known as a distributed dynamo (Brandenburg et al. 1989; Moss et al. 1995).

Barnes et al. (2005) have investigated the link between differential rotation and effective temperature, and hence convective turnover time. They were able to fit an empirical power law to recent observations of a small sample of stars. As the temperature increases, so does the rotational shear. A small number of late-F/early-G type stars have been investigated using Doppler imaging (DI) to determine their differential rotation. HD 171488 (V889 Her) (Marsden et al. 2006), HD 307938 (R58 in IC 2602) (Marsden et al. 2005), HR 1817 (Mengel 2005) and LQ Lup (RX J1508.6−4423) (Donati et al. 2000) have had their differential rotation determined.

Zeeman Doppler imaging (ZDI) (Donati et al. 2003) makes the study of stellar magnetic fields using spectropolarimetry possible

⋆E-mail: waite@usq.edu.au

and offers a window into the underlying magnetic dynamo. ZDI requires high signal-to-noise ratio data as the polarization signature is typically less than 0.1 per cent of the total light intensity (Donati et al. 1997). ZDI only measures the large-scale magnetic fields as small-scale magnetic fields cannot be recovered as the positive and negative magnetic fields within the resolution element are likely to be cancelled out. ZDI has been achieved on a small sample of single, G-type stars such as HD 171488 (V889 Her) (Marsden et al. 2006) and HD 141943 (Marsden et al. 2011a,b).

HD 106506 is a suitable target for DI and ZDI. Henry et al. (1996) identified this star as active while Mason et al. (1998) and Cutispoto et al. (2002) deduced this star as being single. The high-resolution spectroscopic survey of Waite et al. (2005) confirmed this star as a young, rapidly rotating solar-type star. They obtained a rotation rate of $v \sin i \sim 80\,\mathrm{km\,s^{-1}}$, a strong H$\alpha$ chromospheric activity ($\log R'_{\mathrm{H}\alpha} \sim 4.2$) and deformation of the spectral line profiles indicating the presence of large star-spots.

The aim of this investigation is to map the surface of this star with a view to measuring the rotational shear on its surface and to measure and map the magnetic field structure on the surface of this star. This is the third paper in a series that investigates the magnetic field topologies of young Sun-like stars, with HD 141943 being the subject of two earlier papers (Marsden et al. 2011a,b).

2 OBSERVATIONS AND ANALYSIS

Spectropolarimetry of HD 106506 was obtained using the 3.9-m Anglo-Australian Telescope (AAT) over an 11 night period from 2007 March 30 to 2007 April 9. Near-simultaneous *BVR* photometric data were obtained using the University of Louisville's 50-cm telescope at the University of Southern Queensland's Mount Kent Observatory (MKO). MKO is located in Southern Queensland, approximately 160 km south-west of Brisbane.

2.1 *BVR* photometry at the MKO

The University of Louisville 50-cm telescope at MKO is a Corrected Dall–Kirkham design manufactured by Planewave Instruments. *BVR* photometric observations of HD 106506 were made through the standard Cousins *B*, *V* and *R* filters using an SBIG STL-630E with a Kodak KAP-6303E CCD chip that has an array size of 3060 × 2040, 9 μm^2 pixels giving a plate scale of approximately 0.54 arcsec pixel^{-1}. Table 1 shows the journal of observations while a more detailed analysis of this photometric study of HD 106506 has been included in Appendix A.

Table 1. The journal of photometric observations of HD 106506 showing the dates and filters used. The E-5 region (Graham 1982) was observed on 2007 April 11.

UT date	Filters used	UT begin	UT end
2007 April 01	*B*, *V*, *R*	09:12:11	19:03:53
2007 April 02	*B*, *V*, *R*	11:09:03	17:57:21
2007 April 03	*B*, *V*, *R*	09:48:02	18:10:43
2007 April 04	*B*, *V*, *R*	14:33:42	17:59:18
2007 April 05	*B*, *V*, *R*	11:06:02	17:14:08
2007 April 06	*B*, *V*, *R*	09:16:22	18:19:50
2007 April 07	*B*, *V*, *R*	09:13:45	18:13:12
2007 April 08	*B*, *V*, *R*	09:06:57	18:17:01
2007 April 11	*B*, *V*, *R*	10:10:43	13:26:59

Table 2. The journal of spectropolarimetric observations of HD 106506 using the 3.9-m AAT.

UT date	UT begin	UT end[a]	Number of sequences[b]
2007 March 30	09:02:56	13:41:16	5
2007 March 31	08:51:37	13:36:05	5
2007 April 01	08:51:37	13:36:05	5
2007 April 02	08:55:31	13:38:07	5
2007 April 03	09:26:01	16:25:01	3
2007 April 04	08:57:07	12:42:40	2
2007 April 05	10:13:25	14:06:13	4
2007 April 06	09:08:53	12:07:27	2
2007 April 07	08:49:55	13:28:11	5
2007 April 08	10:31:20	11:15:43	1
2007 April 09	09:35:14	11:53:58	2

[a]The UT end is the time when the final exposure for HD 106506 was completed.

[b]Each sequence was of 4 × 600 s exposures. After each exposure, the half-wave Fresnel Rhomb of the SEMPOL polarimeter was rotated between +45° and −45° so as to remove instrumental polarization signals from the telescope and the polarimeter.

2.2 High-resolution spectropolarimetric observations from the AAT

High-resolution spectropolarimetric data were obtained from the AAT using the University College of London Échelle Spectrograph (UCLES) and the Semel Polarimeter (SEMPOL) (Semel 1989; Semel, Donati & Rees 1993; Donati et al. 2003). The detector used was the deep depletion EEV2 CCD with 2048 × 4096, 13.5 μm^2 pixels. UCLES was used with a 31.6 grooves mm^{-1} grating covering 46 orders (orders # 84 – # 129). The central wavelength was 522.002 nm with full wavelength coverage from 437.71 to 681.56 nm. The dispersion of ∼0.004 958 nm at order #129 gave a resolution of approximately 710 00. Observations in the circular polarization signatures (Stokes *V*) consist of a sequence of four exposures. After each exposure, the half-wave Fresnel Rhomb of the SEMPOL polarimeter is rotated between +45° and −45° so as to remove instrumental polarization signals from the telescope and the polarimeter (Donati et al. 2003). A journal of observations is shown in Table 2.

2.2.1 *Spectropolarimetric analysis*

The initial data reduction was completed using the ESpRIT (Échelle Spectra Reduction: an Interactive Tool) software package (Donati et al. 1997, 2003). Preliminary processing involved removing the bias and using a nightly master flat combining typically 20 flat-field exposures. Each stellar spectrum was extracted and wavelength calibrated against a thorium–argon lamp. The mean pixel resolution for the AAT spectra was determined to be 1.689 km s^{-1} pixel^{-1}.

After using ESpRIT, least-squares deconvolution (LSD) was applied to the reduced spectra. LSD combines the information from many spectral lines to produce a single line profile, thereby providing an enormous multiplex gain in the signal-to-noise ratio (S/N) (Donati et al. 1997). The average S/N for a typical Stokes *I* LSD profile was ∼1100 whereas the maximum S/N for the corresponding central order was only ∼50. A G2 line mask created from the Kurucz atomic data base and ATLAS9 atmospheric models (Kurucz 1993) was used during the LSD process.

In order to correct for the minor instrumental shifts in wavelength space, each spectrum was shifted to match the Stokes *I* LSD profile

of the telluric lines contained in the spectra, as was done by Donati et al. (2003) and Marsden et al. (2006). Further information on LSD can be found in Donati et al. (1997).

3 PHOTOSPHERIC AND CHROMOSPHERIC FEATURES

The brightness and magnetic images of HD 106506 were created using the ZDI code of Brown et al. (1991) and Donati & Brown (1997). It utilizes the time-series Stokes *I* and *V* LSD profiles as inputs for the inversion process to produce the brightness and magnetic images. This is an ill-posed problem as there are an infinite number of possible solutions that can be found. The ZDI code uses the maximum-entropy minimization techniques of Skilling & Bryan (1984) to produce an image with the mimimum amount of information required to produce the observed variations in the LSD profile.

3.1 Fundamental parameters of HD 106506

HD 106506 is a G1V star (Torres et al. 2006) with a median visual magnitude of 8.5617 (van Leeuwen 2007), a $B - V$ value of 0.605 and a $V - I$ value of 0.67 [based on the transformed *Hipparcos* and Tycho data, ESA (1997)]. It has a trigonometric parallax of 7.96 ± 0.88 mas (Perryman et al. 1997) giving a distance of 126 ± 14 pc or 410 ± 46l yr. On using this $V - I$ value, the temperature of HD 106506 comes to be approximately 5870 ± 45 K. This was determined using the formulation of Bessell, Castelli & Plez (1998). The absolute magnitude is 3.053 ± 0.244. Using the bolometric corrections listed in Bessell et al. (1998) and the formulation contained within that paper, HD 106506 is estimated to be 2.15 ± 0.26 $R_\odot$. The resulting luminosity of HD 106506 is 4.81 ± 1.2 $L_\odot$. Fig. 1 shows the theoretical tracks of Siess et al. (2000), from which it may be deduced that the star is less than 10 Myr of age and has a mass of between 1.4 and 1.6 $M_\odot$. Table 3 shows the initial parameters that were used in the analysis and the production of the Stokes *I* (intensity) and Stokes *V* magnetic maps.

3.2 Image reconstruction: Stokes *I* Doppler imaging map and surface differential rotation

In order to produce the brightness image of HD 106506, a two-temperature model was used (Collier Cameron 1992), assuming that one temperature was for the quiet photosphere, $T_{\rm phot}$, while the other temperature was for the cooler spots, $T_{\rm spot}$. Synthetic Gaussian profiles were used to represent both the spot temperature and the quiet photosphere temperature. Unruh & Collier Cameron (1995) showed that there is little difference in the resulting maps when using synthetic Gaussian profiles as compared to using profiles obtained from slowly rotating standard stars. A number of authors have followed this formulation, such as Petit, Donati & Collier Cameron (2002), Petit et al. (2004) and Marsden et al. (2005, 2006).

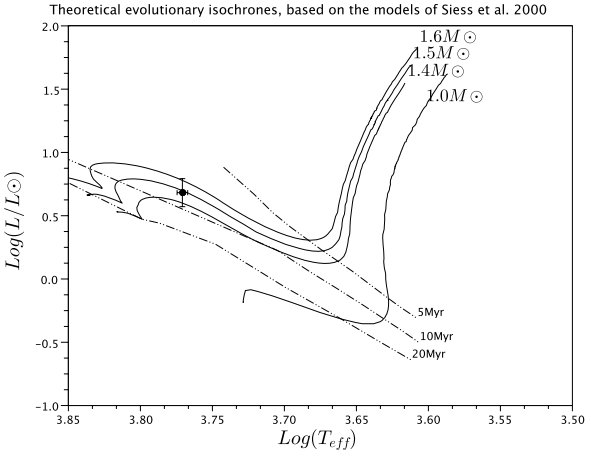

Figure 1. The evolutionary status of HD 106506. This is based on the theoretical models of Siess, Dufour & Forestini (2000).

Table 3. The parameters used to produce the maximum-entropy image reconstruction of HD 106506, including those associated with surface differential rotation.

Parameter	Value
Photometric period	1.416 ± 0.133 d
Equatorial period (using Stokes *I*)	1.39 ± 0.01 d
Inclination angle	65 ± 5°
Projected rotational velocity, $v \sin i$	79.5 ± 0.5 km s^{-1}
Unspotted apparent visual magnitude	8.38
Photospheric temperature, $T_{\rm phot}$	5900 ± 50 K
Spot temperature, $T_{\rm spot}$	4000 ± 50 K
Radial velocity, $v_{\rm rad}$	13.1 ± 0.1 km s^{-1}
Stokes *I*: $\Omega_{\rm eq}$	4.54 ± 0.01 rad d^{-1}
Stokes *I*: $\delta\Omega$	$0.21^{+0.02}_{-0.03}$ rad d^{-1}
Stokes *V*: $\Omega_{\rm eq}$	4.51 ± 0.01 rad d^{-1}
Stokes *V*: $\delta\Omega$	0.24 ± 0.03 rad d^{-1}

The imaging code was used to establish the values of a number of basic parameters, including the star's inclination angle, projected rotational velocity, $v \sin i$ and radial velocity $v_{\rm rad}$. This was achieved by systematically varying each parameter in order to minimize the χ^2 value (see e.g. Jeffers & Donati 2008; Marsden et al. 2005). These key stellar parameters were determined sequentially, first $v_{\rm rad}$, then $v \sin i$ and finally the inclination angle of the star. This sequence was repeated each time additional parameters were modified as a result of the imaging process. The full set of parameters that gave the minimum χ^2 value is shown in Table 3 and was adopted when producing the final Doppler imaging map in Fig. 2(a). By incorporating the photometry from MKO into the imaging process, $T_{\rm phot}$ and $T_{\rm spot}$ were determined by minimizing the deviations between the measured and modelled data in both *V* and *R* bands. The effective photospheric temperature was determined to be 5900 ± 50 K, which is consistent with that calculated based on the photometric colours of the star and using the bolometric corrections of Bessell et al. (1998) within the error bars of both the determinations. The spot temperature was determined to be 4000 ± 50 K. The photospheric-spot temperature difference of 1900 K for this early-G dwarf is consistent with values obtained by other authors such as Marsden et al. (2011a,b, 2005) and supports the relationship developed by Berdyugina (2005). The intensity map with the photometry included is shown in Fig. 2(b).

There have been a number of different ways in which differential rotations have been measured. Reiners & Schmitt (2003) have used a Fourier transform method to derive the parameters for rapidly rotating F-type/early-G type inactive stars. They produce a deconvolved line profile from the stellar spectra and then determine the ratio of the second and first zero of the resulting Fourier transform. This ratio is a measure of differential rotation on the star. However, for active young stars with significant asymmetry within the line profiles, this technique is not as effective. The differential rotation of a star can also be estimated by tracking spot features at different latitudes on the surface of the star. A solar-like differential rotation law, as defined in equation (1), has been applied to a number of

Table 4. A comparison with other late-F/early-G type dwarfs that have had their surface differential rotation measured using Doppler imaging.

Parameter	HD 106506	HD 171488[b,c]	R58 (in IC2602)[d]	LQ Lup[e]	HD 141943[f]
$(B-V)^a$	0.605	0.62	0.61	0.69	0.7
$T_{\rm Photosphere}$ (K)	5900	5800	5800 ± 100	5750 ± 50	5850 ± 100
$T_{\rm Spot}$ (K)	4000	4200	3900 ± 100	4250	3950
Age (Myr)	$\lesssim$10	30–50	35 ± 5	25 ± 10	17
Mass ($M_\odot$)	1.5 ± 0.1	1.06 ± 0.02	1.15 ± 0.02	1.16 ± 0.02	1.3
Radius ($R_\odot$)	2.15 ± 0.26	1.15 ± 0.08	1.18 ± 0.02	1.22 ± 0.02	1.6 ± 0.1
Incl. angle	65 ± 5°	60 ± 5°	60 ± 10°	35 ± 5°	70 ± 10
$v \sin i$ (km s^{-1})	79.5 ± 0.5	37.5 ± 0.1	92 ± 0.5	115 ± 1	35.0 ± 0.5
Stokes *I* measurements					
$\Omega_{\rm eq}$ (rad d^{-1})	4.54 ± 0.01	4.786 ± 0.013	11.165 ± 0.014	20.28 ±0.01	2.86 ± 0.02
$\delta\Omega$ (rad d^{-1})	$0.21^{+0.02}_{-0.03}$	0.402 ± 0.044	0.0815 ± 0.026	0.12 ±0.022	0.24 ± 0.03
Stokes *V* measurements					
$\Omega_{\rm eq}$ (rad d^{-1})	4.51 ± 0.01	4.85 ± 0.05	–	–	2.88 ± 0.02[g] 2.89 ± 0.05[g]
$\delta\Omega$ (rad d^{-1})	0.24 ± 0.03	0.47 ± 0.04	–	–	0.36 ± 0.09[g] 0.45 ± 0.08[g]

[a] *Hipparcos*; [b] Marsden et al. (2006); [c] Jeffers & Donati (2008); [d] Marsden et al. (2005); [e] Donati et al. (2000); [f] Marsden et al. (2011a); [g] Marsden et al. (2011b)

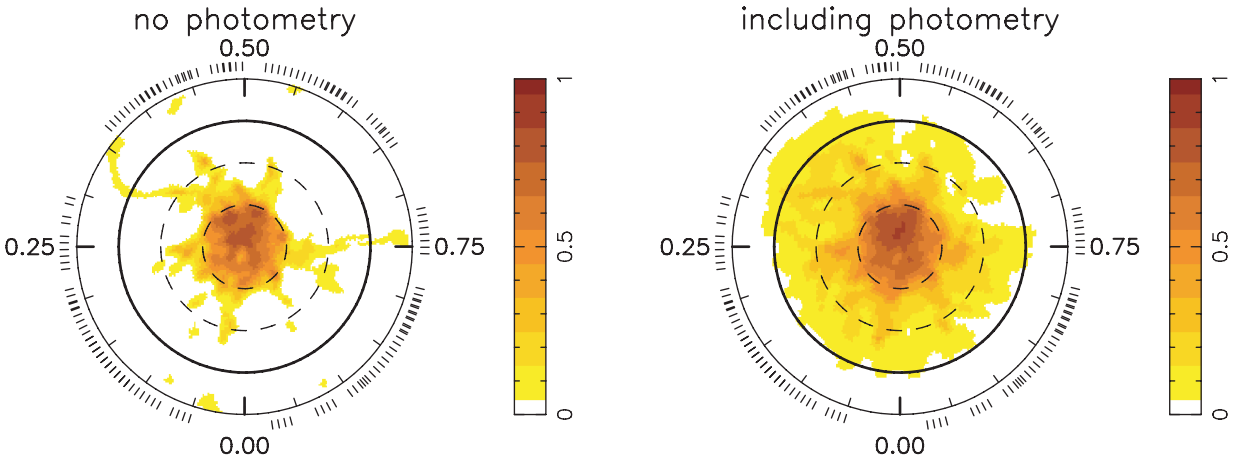

Figure 2. (a) The figure on the left is the maximum entropy map that was generated entirely from the AAT data, with a spot-filling factor of 0.062. (b) The figure on the right is a similar map but including near-simultaneous photometry from the MKO. The spot-filling factor was 0.127. The χ^2 value was set to 0.5 in the modelling process. The images are polar projections extending down to a latitude of −30°. The bold line denotes the equator and the dashed lines are +30° and +60° latitude parallels. The radial ticks indicate the phases at which this star was observed spectroscopically.

solar-type stars (i.e. Donati et al. 2003; Marsden et al. 2005, 2006):

$$\Omega(\theta) = \Omega_{\rm eq} - \delta\Omega \sin^2\theta, \quad (1)$$

where $\Omega(\theta)$ is the rotation rate at latitude θ in rad d^{-1}, $\Omega_{\rm eq}$ is equatorial rotation rate and $\delta\Omega$ is the rotational shear between the equator and the pole. In this work the differential rotation of HD 106506 was measured using a technique that systematically adjusts the differential rotation parameters $\Omega_{\rm eq}$ and $\delta\Omega$ and determines the best fit to the data, by minimizing the difference between the data and the model fits using χ^2 minimization techniques. This technique has been successfully applied to a number of late-F/early-G stars (i.e. Petit et al. 2002, 2004; Barnes et al. 2005; Marsden et al. 2006).

Initially, a fixed spot-filling factor of 0.062, as determined from the reconstructed map, was used and $\Omega_{\rm eq}$ and $\delta\Omega$ were considered to be free parameters. The magnitude of the differential rotation was then determined by fitting a paraboloid to the reduced χ^2 values. The minimum value for $\Omega_{\rm eq}$ was determined to be 4.54 ± 0.01 rad d^{-1} and $\delta\Omega$ was $0.21^{+0.02}_{-0.03}$ rad d^{-1}. By incorporating the differential rotation into the maximum-entropy image reconstruction, the resulting map is shown in Fig. 2, along with the model fits to the LSD profiles in Fig. 3. The errors for the value of the differential rotation were established by varying both the spot filling factor and the inclination angle by ± 10 per cent and determining $\Omega_{\rm eq}$ and $\delta\Omega$ respectively. When varying the inclination angle, the associated multiplication factors were redetermined and the resulting spot filling factor was found to match the new angle by minimising the χ^2 value. The reduced χ^2 values for the various $\Omega_{\rm eq}$ and $\delta\Omega$, along with the associated error ellipse, are shown in Fig. 4.

Fig. 2 shows, on the left, the resulting maximum-entropy image reconstructed map generated using the spectroscopic data obtained at the AAT. The right-hand side of this figure is the reconstructed image created using both the spectroscopic data and the near-simultaneous photometric data obtained at the MKO. The

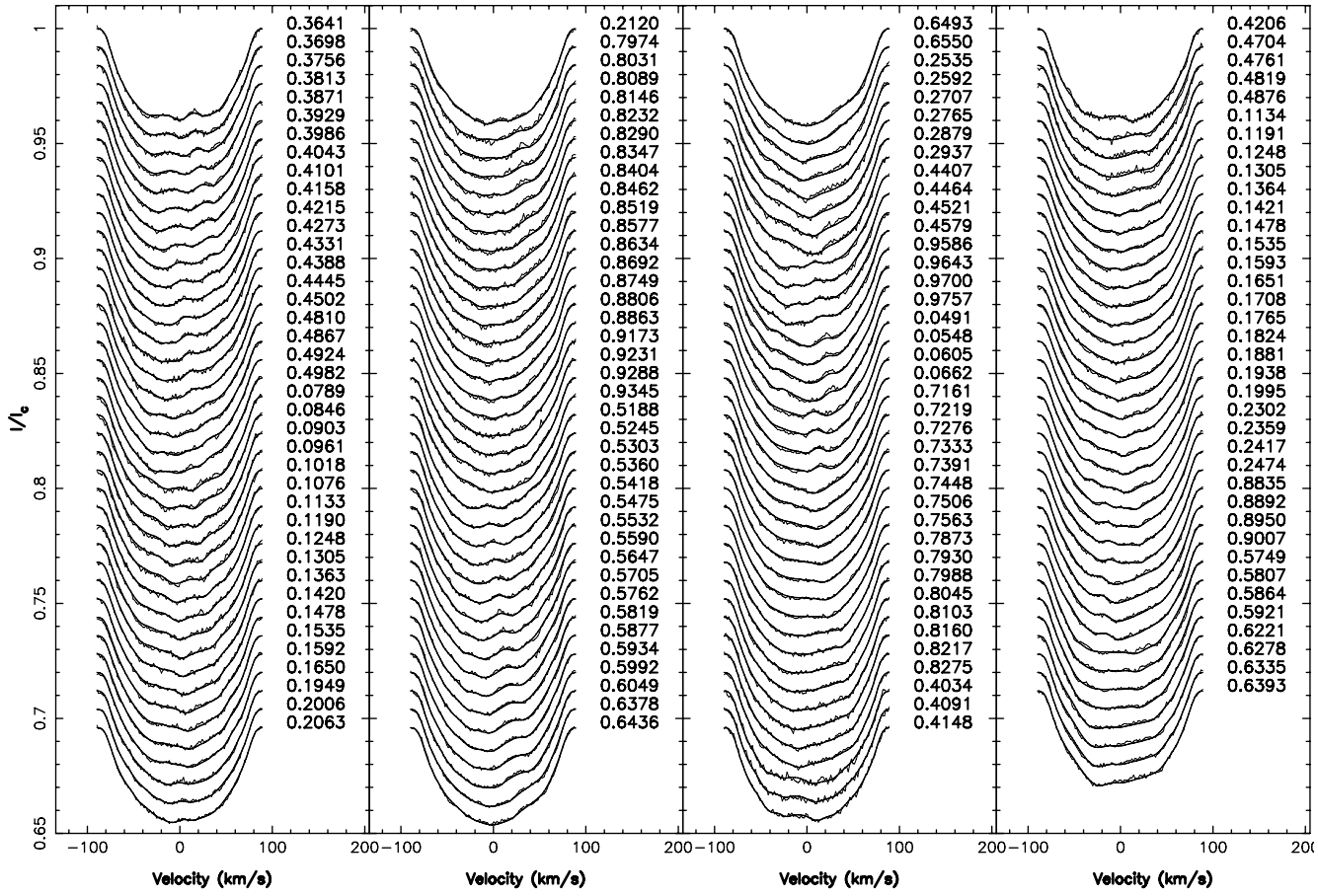

Figure 3. The maximum-entropy fits to the LSD profiles for HD 106506 with both photometry and surface differential rotation incorporated into the analysis. The thick lines represent the modelled lines produced by the Doppler imaging process whereas the thin lines represent the actual observed LSD profiles. Each successive profile has been shifted down by 0.005 for graphical purposes. The rotational phases at which the observations took place are indicated to the right of each profile.

photometry data have enhanced the lower-latitude features. In each map, an equatorial period of 1.39 d has been used, which was established during the differential rotation analysis and the epoch was set to 245 4194.936 423 61, which was the middle of the observation run.

Fig. 5 shows the *V* and *R* light curves coupled with the maximum-entropy fits that were used to produce the enhanced DI map. Fig. 3 shows the model profiles overlayed on the measured LSD profiles. The model profiles include the differential rotation parameters. The dynamic spectrum of the residuals between the observed and modelled profiles is shown in Fig. 6. It appears that the Doppler imaging process, combined with incorporating the differential rotation parameters, has removed the majority of the large-scale features with only a small amount of structure still apparent in this dynamic spectrum.

3.3 Zeeman Doppler imaging: magnetic features on the surface of HD 106506

The modelling strategy of Donati & Brown (1997) was used to construct the magnetic field topology on HD 106506. This involved utilizing the spherical harmonic expansions of the surface magnetic field as implemented by Donati et al. (2006). The spherical harmonic expansion $l_{\max} = 40$ was selected as this was the minimum value for which any further increase resulted in no further changes in the magnetic topologies.

Initially, a poloidal plus toroidal field was assumed, then the images were created by fitting the data to within the noise level and resulted in a mean field strength of 68.84 G. A similar approach to measuring the differential rotation parameters was used for the Stokes *I* (brightness) features. When considering these magnetic features, the equatorial rotation rate $\Omega_{\rm eq}$ was $4.51 \pm 0.01\,{\rm rad\,d^{-1}}$, with a photospheric shear $\delta\Omega$ of $0.24 \pm 0.03\,{\rm rad\,d^{-1}}$. This implies that the equatorial rotation period was 1.38 d with a shear approximately four times that of the solar value.

The reconstructed magnetic fields are shown in Fig. 7. The fits to the Stokes *V* LSD profiles are given in Fig. 8.

3.4 Chromospheric features: prominences

The Hα line has been extensively used as a indicator of chromospheric activity (e.g. Thatcher & Robinson 1993).

A mean Hα spectral line for HD 106506 was generated from all the Hα profiles obtained during the observing run. Each individual spectrum was then subtracted from the mean Hα line, and dynamic spectra were then produced. Chromospheric features were observed at phases ∼0.15 and ∼0.75. This is shown in Fig. 9.

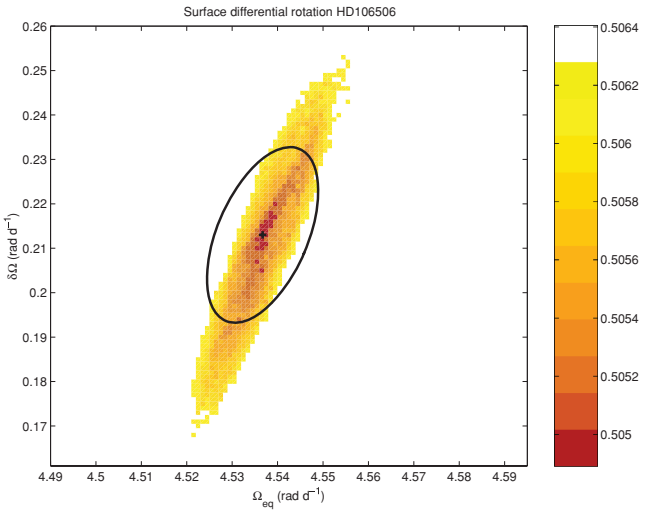

Figure 4. Surface differential rotation χ^2 minimization for HD 106506. The image shows the reduced χ^2 values from the maximum-entropy Doppler imaging code for a fixed spot coverage of 0.062 and an inclination angle of 65°. The darker regions correspond to lower χ^2 values. The image scale projects $\pm 7\sigma$ on to the axes in both Ω_{eq} and $\delta\Omega$. The ellipse superimposed demonstrates the error for the value of the differential rotation and was determined by varying both the star's inclination and spot-filling factors by ± 10 per cent and determining Ω_{eq} and $\delta\Omega$.

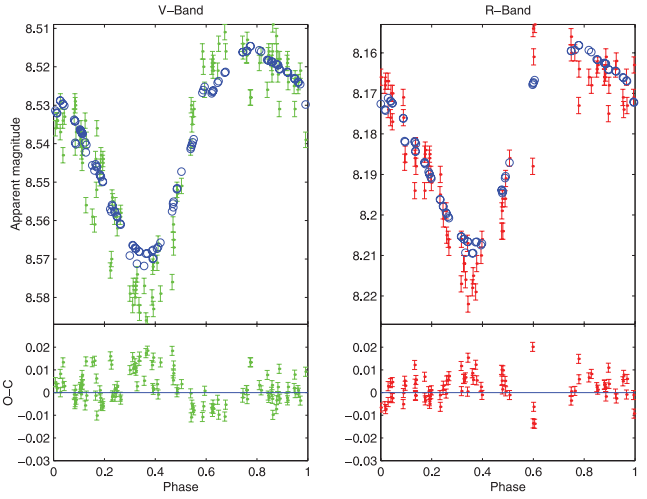

Figure 5. The photometric light curves for both V filter and R filter (the points with error bars) coupled with the maximum-entropy fits (circles) for HD 106506. The bottom graph in each panel shows the Observed − Calculated values.

4 DISCUSSION

4.1 Spot features and surface differential rotation

Spectroscopic and photometric observations were used to produce the spot occupancy map shown in Fig. 2. Photometry is very useful at extracting out the lower latitude features [Jeffers, Barnes & Collier Cameron (2002)] but is not sensitive to the high-latitude features as these are always in view, whereas the spectroscopy extracts the higher latitude features (Unruh & Collier Cameron 1997)

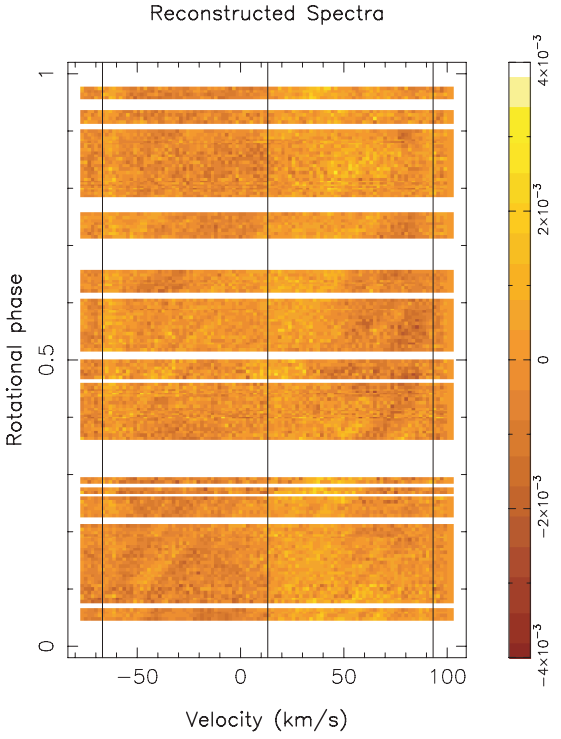

Figure 6. Dynamic spectra of the residuals between the observed and modelled LSD profiles, including differential rotation. The spectra are centred on the radial velocity of HD 106506. The three lines on the image shows the centre of the line profile (centre line) and the rotational broadening of the line profile (outer lines), which is 79.5 km s^{-1}.

but cannot discriminate lower latitude features at latitudes $\lesssim 30°$. Hence to get a more complete picture of the stellar image, both photometric and spectroscopic data need to be incorporated into the imaging process. Using the Stokes I spectroscopic information coupled with the photometry, the spot occupancy map, as shown in Fig. 2, shows low-latitude to mid-latitude spots, and the predominant polar spot. This variation of spot occupancy with stellar latitude using spectroscopy alone and inclusive of the photometry is shown in Fig. 10. The fractional spottedness is defined in equation (2):

$$F(\theta) = S(\theta)\cos(\theta)\mathrm{d}\theta/2, \qquad (2)$$

where $F(\theta)$ is the fractional spottedness at latitude θ, $S(\theta)$ is the average spot occupancy at latitude θ and $\mathrm{d}\theta$ is the latitude width of each latitude ring.

The exact reasons why rapidly rotating stars have polar spots are still not fully understood. One theory (Schüssler et al. 1996; Buzasi 1997; Deluca, Fan & Saar 1997) postulates that high-latitude, but not truly polar, spots are a result of the increased Coriolis effect, due to the rapid rotation, which may have the effect of deflecting the spot features to higher latitudes as they erupt through the star's convection zone. An alternative hypothesis (Schrijver & Title 2001; Kitchatinov & Rüdiger 1999) involves the transport of flux through the process of meridional flow. It is yet to be determined whether the polar spots on young solar-type stars are formed at high latitudes by the strong Coriolis effect in these rapidly rotating stars, or formed at low latitudes and pushed poleward by subsurface meridional flows. Nevertheless, the issue can be clarified by long-term monitoring of the spot topology of these stars, because meridional flows should be

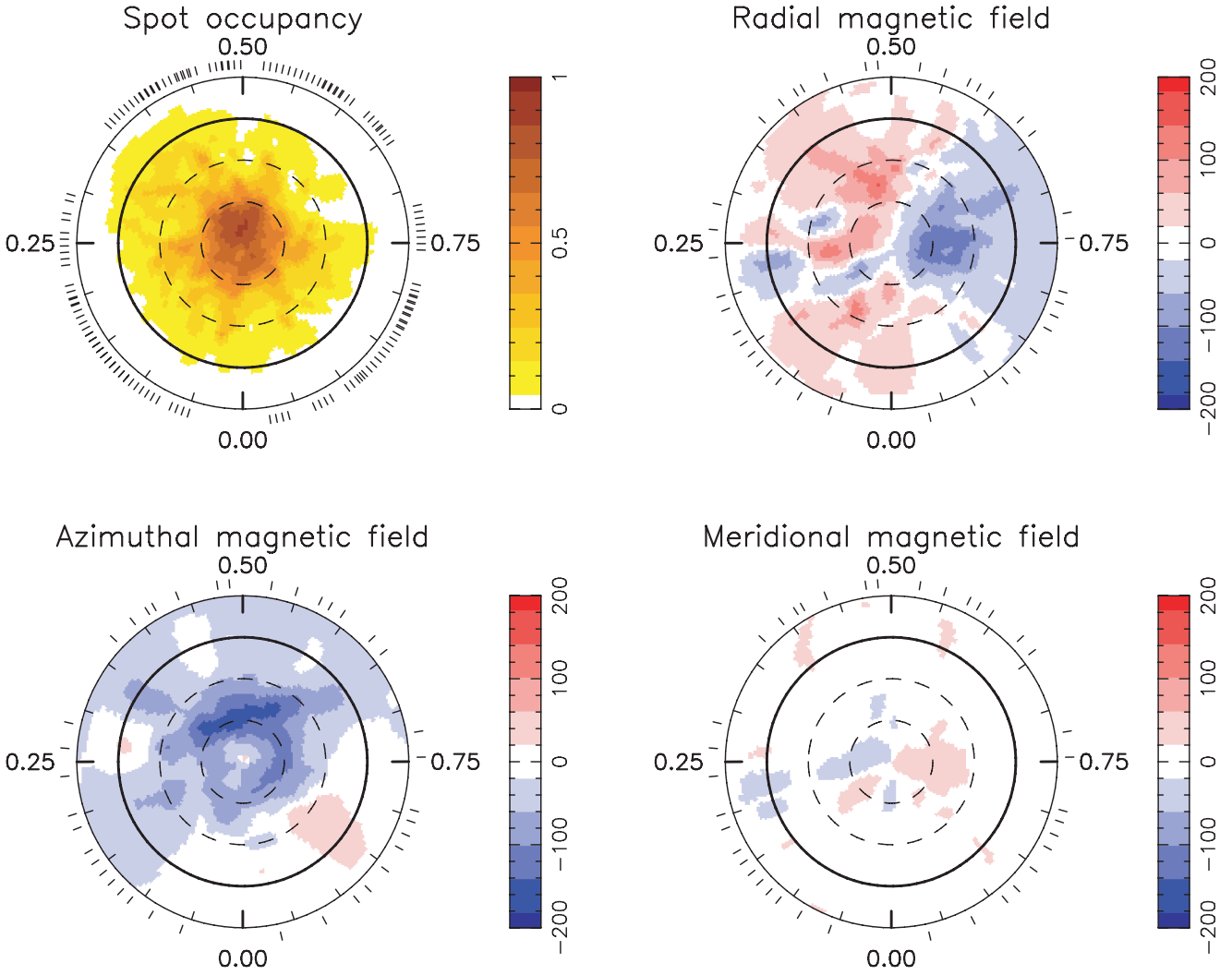

Figure 7. The maximum-entropy brightness and magnetic image reconstructions for HD 106506. These maps are polar projections extending down to −30°. The bold lines denote the equator and the dashed lines are +30° and +60° latitude parallels. The radial ticks indicate the phases at which this star was observed spectroscopically. The scale of the magnetic images is in Gauss. The brightness image (top left-hand image) has a spot-filling factor of ∼0.127 (or 12.7 per cent) and is a combination of both spectroscopic and photometric data. The magnetic images have a field modulus of 68.84 G. Differential rotation, as measured using the Stokes *V* profiles, has been incorporated into the analysis.

detectable as poleward drifts in star-spot features over time. Weber, Strassmeier & Washuettl (2005) have reported tentative evidence for large poleward meridional flows on early-K giants, but to the best of our knowledge, such an effect has yet to be detected for young solar-type stars.

These reconstructed images are consistent with those obtained in other Doppler images produced for young, single, rapidly rotating solar-type stars. The photometry enabled more of the low-latitude features to be recovered, as was done for the star R58 (in IC 2602) by Marsden et al. (2005).

When using the Stokes *I* information HD 106506 was found to have a photospheric shear of $0.21^{+0.02}_{-0.03}$ rad d^{-1} with the equator lapping the poles every $\sim 30^{+5}_{-3}$ d. When compared with the Sun's value of $\delta\Omega = 0.055$ rad d^{-1}, with a lap time of 115 d, this young pre-main sequence solar-type star has a shear roughly four times greater than that of the Sun. This result is consistent with the relationship determined by Barnes et al. (2005) that differential rotation is dependent on spectral class (surface temperature), with M-dwarfs rotating almost as a solid body through to early-G dwarfs exhibiting a strong rotational shear. However, Marsden et al. (2006) and Jeffers & Donati (2008) have found that the early G-dwarf HD 171488 (V889 Her) has a photospheric shear up to seven times the solar value. So why do these two stars that exhibit similar surface temperature properties have vastly different photospheric shear? One possible reason is that HD 106506 is a more distended star, with a larger convective zone when compared with HD 171488. Being a younger star, it is probably still contracting down to the main sequence. But it is still unclear why HD 171488 should have such a large $\delta\Omega$ and perhaps it is the convective zone depth and the rate at which that zone is turned over that are more important than the surface temperature (hence spectral type). We show HD 106503, along with HD 141943 (Marsden et al. 2011b), HD 171488 (Marsden et al. 2006) and additional data from Jeffers & Donati (2008), on the graph of $\delta\Omega$ versus effective temperature produced by Barnes et al. (2005) in Fig. 11. HD 106506 supports the power law developed by Barnes et al. (2005). Table 4 shows a comparison of the late-F/early-G type dwarfs that have had their surface differential rotation measured using Doppler imaging.

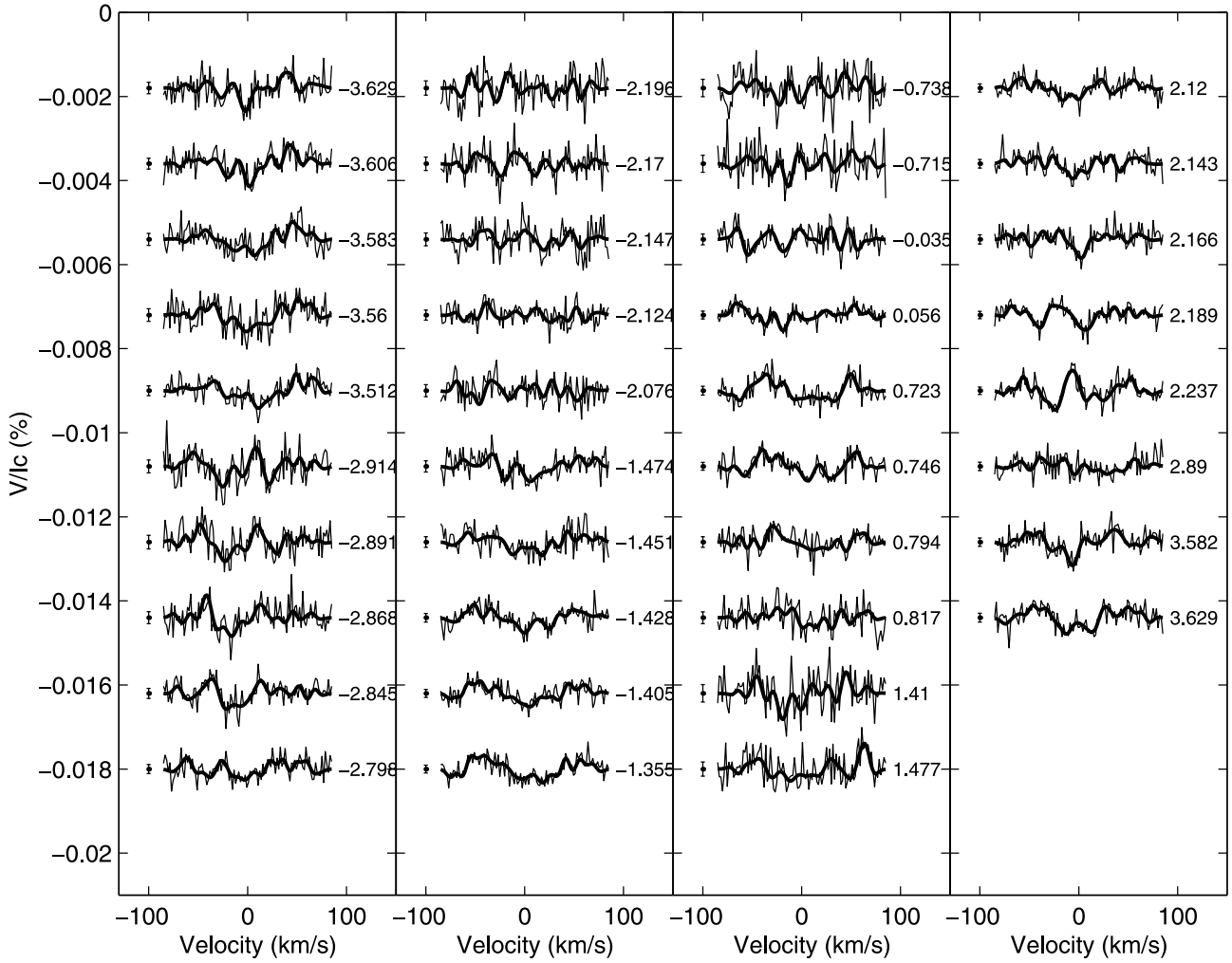

Figure 8. The maximum-entropy fits to the Stokes *V* LSD profiles for HD 106506 with surface differential rotation, as measured using the Stokes *V* profiles, incorporated into the analysis. The thick lines represent the modelled lines produced by the Zeeman Doppler imaging process whereas the thin lines represent the actual observed LSD profiles. Each successive profile has been shifted down by 0.002 for graphical purposes. The error bar on the left of each profile is plotted to $\pm 0.5\sigma$. The rotational phases, in terms of the number of rotational cycles, at which the observations took place are indicated to the right of each profile.

4.2 Magnetic topology

The reconstructed magnetic fields are shown in Fig. 7 and the fits to the Stokes *V* LSD profiles are given in Fig. 8. Magnetic features in both the azimuthal and radial magnetic fields extend from low-latitude to high-latitude features. As discussed by Donati et al. (2003), the radial component may be interpreted to be representative of the poloidal component while the azimuthal component may be considered as representative of the toroidal component of the large-scale dynamo field. The strong azimuthal ring around the star is similar to those observed on other stars such as HD 171488 (Jeffers & Donati 2008). However, the azimuthal ring on HD 106506 is of different polarity from those observed on other stars, such as HD 141943 (Marsden et al. 2011a). This is unlikely to be due to instrumental polarization as the data for HD 106506 were obtained with the same instrumental set-up and at the same time as HD 141943.

The azimuthal ring of magnetic field is consistent with the wreathes of magnetic fields theorized by Brown et al. (2010), except at a much higher latitude. Their three-dimensional MHD models found that stars with increased rotation rate (up to three times that of the Sun) could produce self-generating wreathes of azimuthal field without the need for an interface layer. One can speculate that the increased rotation rate of HD 106506 could be deflecting the wreathes of magnetic fields to much higher latitudes, as seen in Fig. 7.

Donati & Landstreet (2009) found that upon increasing the rotation rate of a star, the toroidal component of the surface magnetic field dominates over the poloidal component of that field. The magnetic field on HD 106506 is predominantly toroidal with approximately 70 ± 3 per cent of the magnetic energy being toroidal magnetic energy. This is similar to the toroidal field being the dominant field of HD 171488 (Marsden et al. 2006; Jeffers & Donati 2008), AB Dor and LQ Hya (Donati et al. 2003). Like HD 171488, this field is quite complex, much more so than what is operating the Sun. Considering the toroidal component, an octopole field dominates with approximately 37 ± 9 per cent of the magnetic energy whereas the dipole field contains only 18 ± 5 per cent and a quadrupole field containing approximately 16 ± 7 per cent of the magnetic energy. This is in contrast to the poloidal field where the respective components are roughly equal between a dipole (10 ± 2 per cent), quadrupole (11 ± 2 per cent) and octopole field

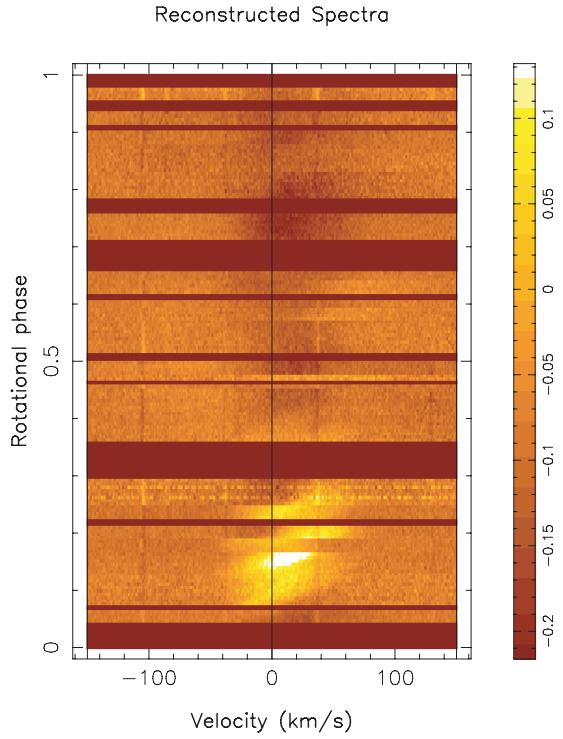

Figure 9. This figure shows a chromospheric features observed on HD 106506. The chromosphere is more dense at phase of ∼0.15. There also appears to be an area at ∼0.75 where the chromosphere is less dense.

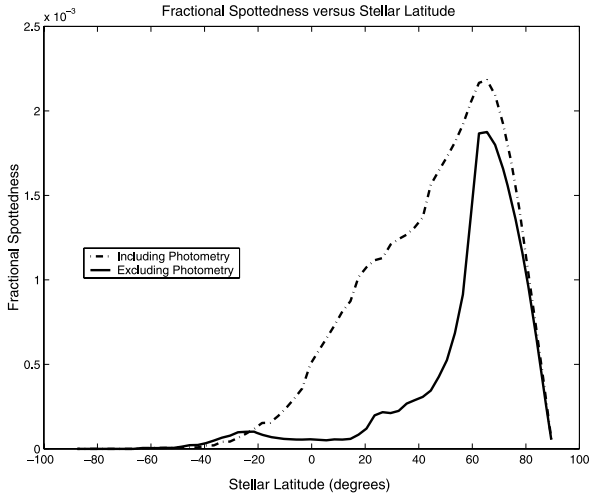

Figure 10. The fractional spottedness versus stellar latitude for HD106506 with and without photometry included in the imaging process. The fractional spottedness is based on the average spot occupancy at each longitude and is defined in equation (2). The photometry is very useful at extracting out the lower latitude features whereas the spectroscopy extracts the higher latitude features.

(10 ± 1 per cent). This would indicate that a much more complex dynamo is operating on HD 106506 and is similar to that on other young, Sun-like stars. In addition, the toroidal field was predominantly axisymmetric (95 ± 2 per cent) whereas the poloidal field tended to be more non-axisymmetric (65 ± 7 per cent). This is consistent with the observations of Donati & Landstreet (2009) and Marsden et al. (2011a) where stars with significant toroidal fields often have non-axisymmetic poloidal fields. The error esti-

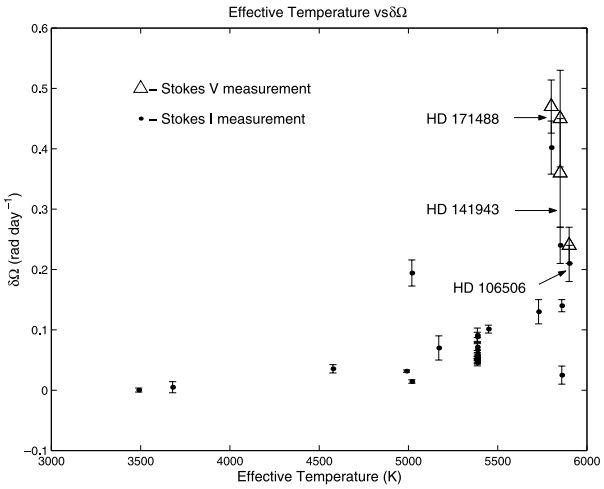

Figure 11. This shows a graph of $\delta\Omega$ versus effective surface temperature, as originally produced by Barnes et al. (2005). The data for HD 171488 (Marsden et al. 2006), HD 141943 (Marsden et al. 2011a) and HD 106506 have been added to this graph. HD 106506 supports the power law developed by Barnes et al. (2005) whereas HD 171488 and HD 141943 appear not to support this relationship.

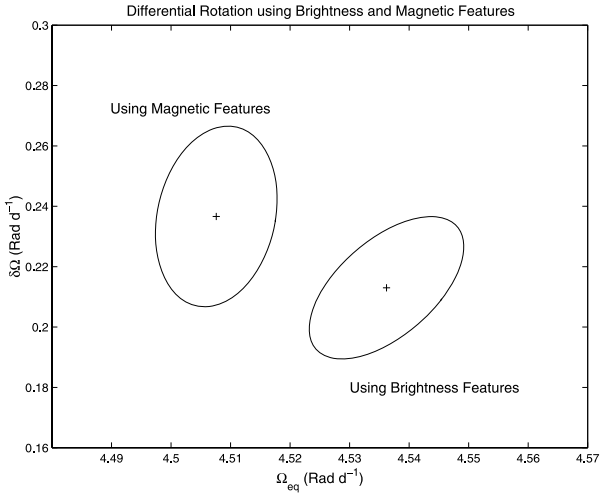

Figure 12. This shows a graph of the error ellipses for the differential rotation measurements for both the Stokes *I* (on the right) and the Stokes *V* (left). These error ellipses were generated by varying some of the stellar parameters, including the star's inclination (±10°) and the Stokes *I* spot coverage or the Stokes *V* global magnetic field (±10 per cent).

mates on these measures were obtained by varying a range of stellar parameters such as inclination, radial velocity, $\Omega_{\rm eq}$, $\delta\Omega$, period and $v \sin i$. Hence these may be referred to as a *variation* bar, which is analogous to an error bar except that the measurement indicates the variation found by this method.

When measuring the differential rotation using the magnetic features, the equatorial rotation rate $\Omega_{\rm eq}$ was 4.51 ± 0.01 rad d^{-1}, with a photospheric shear $\delta\Omega$ of 0.24 ± 0.03 rad d^{-1}. The comparison with those parameters found using the Stokes *I* information is shown in Fig. 12. However, this difference in the $\delta\Omega$ values are within the error bars of the two measurements. When compared with the differences observed on other stars of similar spectral type such as HD 141943 (Marsden et al. 2011b), these features may be anchored at similar depths in the convective zone, unlike HD 141943 which may be anchored at different depths of the convective zone. However,

this conclusion must be treated with caution until further Stokes *V* data are obtained for this star.

4.3 Hα emission

Fig. 9 shows a bright-spot in this dynamic profile at ∼0.15 phase. This is where the chromosphere is much denser as a result of an increase in temperature in that local region. There appears to be a reduced emission at ∼0.75 phase as well. These variations in Hα emission lie within the stellar velocity profile and hence arise from regions close to the stellar surface. We thus interpret these Hα variations in terms of prominences more akin to solar prominences than the more extended features known to exist at the corotation radius of other active solar-type stars, such as LQ Lup (Donati et al. 2000).

5 CONCLUSIONS

In this paper, reconstructed brightness and magnetic images of the young solar-type star HD 106506 have been presented. The brightness image shows low-latitude to mid-latitude features coupled with a predominant polar spot. This is very similar to many of rapidly rotating solar-type stars. The magnetic images reveal regions of azimuthal field near the stellar surface that suggest that the dynamo mechanism may be occurring entirely in the convective zone and close to the surface of the star itself. The photospheric shear for HD 106506 supports the findings of Barnes et al. (2005) that effective temperature is the dominant factor in determining the level of surface differential rotation. However, the reason why such a relation exists remains unclear.

ACKNOWLEDGMENTS

The authors would like to thank the technical staff at the AAT for their helpful assistance during the acquisition of the spectroscopic data. Thanks are also due to Dr John Kielkopf (UofL) for his expertise in developing the University of Louisville Telescope at MKO and to Roger McQueen for taking some of the photometric data. We thank the anonymous referee for their diligence and many helpful comments that led to substantial improvements to this paper. This project is supported by the Commonwealth of Australia under the International Science Linkages programme. This project used the facilities of SIMBAD, HIPPARCOS and IRAF. This research has made use of NASA's Astrophysics Data System.

REFERENCES

Barnes J. R., Collier Cameron A., Donati J.-F., James D. J., Marsden S. C., Petit P., 2005, MNRAS, 357, L1
Belserene E. P., 1988, S&T, 76, p. 288
Berdyugina S. V., 2005, Living Rev. Solar Phys., 2, 8
Bessell M. S., Castelli F., Plez B., 1998, A&A, 333, 231
Brandenburg A., Krause F., Meinel R., Moss D., Tuominen I., 1989, A&A, 213, 411
Brown S. F., Donati J.-F., Rees D. E., Semel M., 1991, A&A, 250, 463
Brown B. P., Browning M. K., Brun A. S., Miesch M. S., Toomre J., 2010, ApJ, 711, 424
Buzasi D. L., 1997, ApJ, 484, 855
Collier Cameron A., 1992, in Byrne P. B., Mullan D. J., eds, Lecture Notes Phys. Vol. 397, Surface Inhomogeneities on Late-type Stars. Springer, Berlin, p. 33
Cutispoto G., Pastori L., Pasquini L., de Medeiros J. R., Tagliaferri G., Andersen J., 2002, A&A, 384, 491
DeLuca E. E., Fan Y., Saar S. H., 1997, ApJ, 481, 369
Donati J.-F., Brown S. F., 1997, A&A, 326, 1135
Donati J.-F., Landstreet J. D., 2009, ARA&A, 47, 333
Donati J.-F., Semel M., Carter B. D., Rees D. E., Collier Cameron A., 1997, MNRAS, 291, 658
Donati J.-F., Mengel M., Carter B. D., Marsden S., Collier Cameron A., Wichmann R., 2000, MNRAS, 316, 699
Donati J.-F. et al., 2003, MNRAS, 345, 1145
Donati J.-F. et al., 2006, MNRAS, 370, 629
ESA, 1997, The Hipparcos and Tycho Catalogues, ESA SP-1200. ESA, Noordwijk
Graham J. A., 1982, PASP, 94, 244
Henry T. J., Soderblom D. R., Donahue R. A., Baliunas S. L., 1996, AJ, 111, 439
Jeffers S. V., Donati J.-F., 2008, MNRAS, 390, 635
Jeffers S. V., Barnes J. R., Collier Cameron A., 2002, MNRAS, 331, 666
Kitchatinov L. L., Rüdiger G., 1999, A&A, 334, 911
Kurucz R. L., 1993, CDROM #13 (ATLAS9 atmospheric models) and CDROM #18 (ATLAS9 and SYNTHE routines, spectral line database)
Marsden S. C., Waite I. A., Carter B. D., Donati J.-F., 2005, MNRAS, 359, 711
Marsden S. C., Donati J.-F., Semel M., Petit P., Carter B. D., 2006, MNRAS, 370, 468
Marsden S. C. et al., 2011a, MNRAS, doi:10.111/j.1365-2966.2011.18272.x
Marsden S. C. et al., 2011b, MNRAS, doi:10.111/j.1365-2966.2011.18367.x
Mason B. D., Henry T. J., Hartkopf W. I., Ten Brummelaar T., Soderblom D. R., 1998, AJ, 116, 2975
Mengel M. W., 2005, M.Phil thesis, Univ. Southern Queensland
Moss D., Barker D. M., Brandenburg A., Tuominen I., 1995, A&A, 294, 155
Perryman M. A. C. et al., 1997, A&A, 323, L49
Petit P., Donati J.-F., Collier Cameron, 2002, MNRAS, 334, 374
Petit P. et al., 2004, MNRAS, 351, 826
Reiners A., Schmitt J. H. M. M., 2003 A&A, 412, 813
Schrijver C. J., Title A. M., 2001, ApJ, 551, 1099
Schüssler M., Caligari P., Ferriz-Mas A., Solanki S. K., Stix M., 1996, A&A, 314, 503
Semel M., 1989, A&A, 225, 456
Semel M., Donati J.-F., Rees D. E., 1993, A&A, 278, 231
Siess L., Dufour E., Forestini M., 2000, A&A, 358, 593
Skilling J., Bryan R. K., 1984, MNRAS, 211, 111
Stetson P. B., 1990, PASP, 102, 932
Thatcher J. D., Robinson R. D., 1993, MNRAS, 262, 1
Torres C. A. O., Quast G. R., da Silva L., de la Reza R., Melo C. H. F., Sterzik M., 2006, A&A, 460, 695
Unruh Y. C., Collier Cameron A., 1995, MNRAS, 273, 1
Unruh Y. C., Collier Cameron A., 1997, MNRAS, 290, L37
van Leeuwen F., 2007, A&A, 474, 653
Waite I. A., Marsden S. C., Carter B. D., Mengel M., 2005, PASA, 22, 29
Weber M., Strassmeier K. G., Washuettl A., 2005, Astron. Nachr., 326, 287

APPENDIX A: *BVR* PHOTOMETRY AT MKO: 2005 AND 2007

The IRAF package was used for the reduction and analysis of the data. The CCD frames had the dark current removed (that also contained the Bias information) and were flat-fielded using a nightly master flat-field, which was a combination of nine dome flat-fields. To produce a single data point, three images obtained through each filter of each star field were averaged, using IMCOMBINE, to produce an image with improved signal-to-noise ratio from which the magnitude of all the programme stars were measured. The stars in the frame were found using DAOFIND, and simple aperture photometry was done using DAOPHOT. The sky background was determined and removed using the mode of an annulus of 10-pixel radius around the star. The curves of growth method (Stetson 1990) was used to

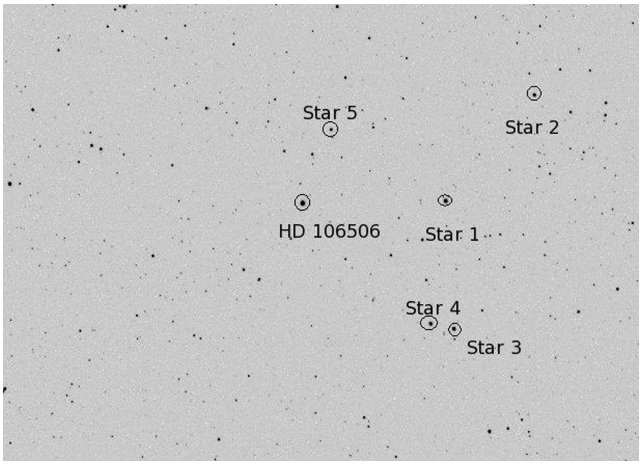

Figure A1. The area surrounding HD 106506, showing five of the brighter stars, were used in the determination of the period. The stars' names are shown in Table A2 in Appendix A.

determine the aperture size that would be used to determine the magnitude of each of the stars in the field.

A1 Standardization of comparison stars: 2005 July 25

BVR photometry was conducted at MKO in 2005 in order to determine the photometric colour of HD 106506 and the other nearby stars within the field of view. Fig. A1 shows the target star; five comparison stars within the same field of view are indicated. Several *BVR* photometric observations of the standard stars in Graham's E regions (Graham 1982) were made. The O'Mara telescope used for this procedure comprises a 35-cm Schmidt–Cassegrain optics; an SBIG STL-1301E CCD camera with 1280 × 1014, 16 μm^2 pixels; and a Paramount ME mount. The three regions used were the E-5 (Stars A, O, U, S, V, Y, c), E-6 (Stars 98, M, P, X, W) and E-7 (Stars M and S) regions. The routines found in the PHOTCAL package in IRAF were used to determine both the transformation coefficients and the magnitude of the stars, including HD 106506. There were three images obtained through each filter of the star fields and then averaged using IMCOMBINE, to produce a single image from which the magnitude of all the standard stars and the program stars were measured. The following transformation equations were solved using the FITPARAM task in IRAF:

$$m_b = B + b_0 + b_1 X_b + b_2(B - V), \quad \text{(A1)}$$

$$m_v = V + v_0 + v_1 X_v + v_2(B - V), \quad \text{(A2)}$$

$$m_r = R + r_0 + r_1 X_r + r_2(V - R), \quad \text{(A3)}$$

where *B, V* and *R* are listed magnitudes of the standard stars in Graham (1982). The instrumental magnitudes, as measured by DAOPHOT were m_b, m_v and m_r. The zero-points are b_0, v_0 and r_0, while b_1, v_1 and r_1 are the extinction coefficients and b_2, v_2 and r_2 are the colour-correction coefficients. The values determined for the coefficients are given in Table A1 and the results are shown in Table A2.

Table A1. Transformation coefficients for the 2005 July 25 photometry at MKO. The associated errors, rms fit and χ^2 value for each filter have been included.

n	b_n	v_n	r_n
0	−3.217	−3.506	−3.709
	±0.14	±0.13	±0.12
1	0.311	0.144	0.134
	±0.11	±0.09	±0.10
2	−0.154	0.065	0.020
	±0.12	±0.06	±0.14
χ^2	0.103	0.060	0.023
rms fit	0.021	0.019	0.011

Table A2. The *BVRI* information for HD 106506 and the comparison stars. Graham's E regions (Graham 1982), E-5, E-6 and E-7, were used to standardize these stars and the data were processed using the routines in PHOTCAL found in IRAF. The data were obtained on 2005 July 25 and a sample image, with the star number included, is shown in Fig. A1.

Star	Star's name	*V*	*BV*	*VR*
Target	HD 106506	8.463	0.594	0.356
Star 1	HD 106507	9.152	−0.024	0.044
Star 2	TYC 8979-979-1	10.108	0.100	0.101
Star 3	TYC 8978-1180-1	10.003	1.083	0.584
Star 4	HD 106417	10.133	1.015	0.558
Star 5	TYC 8978-5479-1	10.948	0.203	0.165

A2 *BVR* broad-band photometric observations from MKO: 2007

Table 1 shows a log of data obtained during the observation run in 2007. The aperture size selected had a pixel radius of 15, giving an aperture radius of approximately 8 arcsec. On April 11, several observations of the standard stars in Graham's E-5 regions (Graham 1982) were made so as to place HD 106506 on the standard magnitude scale. The stars used were A, O, U, S. The routines found

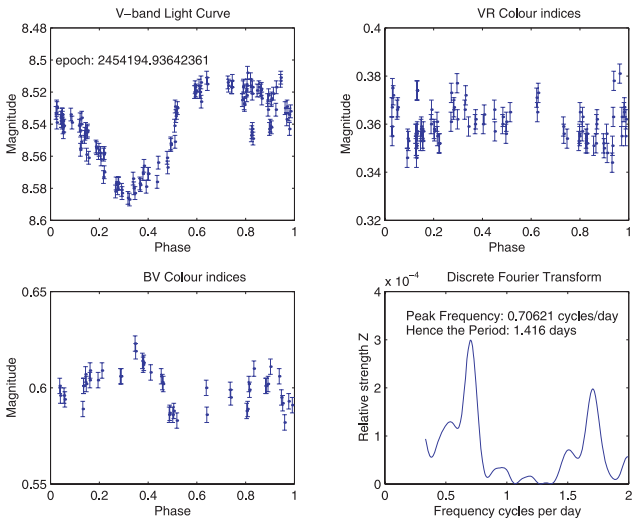

Figure A2. The top-left panel shows the *V*-band light curve for HD 106506, with the phase referenced to epoch = 245 3543.936 423 61-d which coincided approximately with the middle of the AAT run. The $B - V$ and $V - R$ colour light curves are also shown. The bottom-right panel shows the discrete Fourier transform, which is interpreted in terms of a rotation period of 1.416 d.

in the PHOTCAL package in IRAF were used to determine both the transformation coefficients and the magnitude of the stars, including HD 106506. There were three images obtained through each filter of each star field and these were averaged, using IMCOMBINE, to produce an image with improved signal-to-noise ratio from which the magnitude of all the standard stars and the program stars were measured.

A3 Period determination in 2007

The rotational period was determined using discrete Fourier transforms (DFT), using the algorithm as explained by Belserene (1988). The five brighter stars were selected as possible comparison stars and the period was determined for each in B, V and R bands. The average period was determined to be 1.416 ± 0.133 d, and was consistent with all the comparison stars in B, V and R bands. The error was determined by finding the full width at half-maximum of the DFT line profile. Fig. A2 shows the phased folded light curve for the V band as well as the $B - V$ and $V - R$ colour indices. The power spectrum is also shown as generated by the DFT algorithm. Graham's E-5 region, coupled with the five stars previously standardized, was used to place HD 106506 on to the Cousins magnitude system.

This paper has been typeset from a TEX/LATEX file prepared by the author.